



Trans. Nonferrous Met. Soc. China 28(2018) 2028-2043

Transactions of Nonferrous Metals Society of China

www.tnmsc.cn



Microstructure evolution and corrosion behavior of Fe–Al-based intermetallic aluminide coatings under acidic condition

Wen-juan LIU¹, Yu WANG², Hong-bin GE¹, Li LI³, Yi DING¹, Ling-gang MENG⁴, Xing-guo ZHANG⁴

- 1. College of Materials Science and Engineering, Nanjing Tech University, Nanjing 210009, China;
- 2. School of Materials Science and Engineering, North University of China, Taiyuan 030051, China;
- 3. College of Chemistry and Molecular Engineering, Nanjing Tech University, Nanjing 211800, China;
- 4. School of Materials Science and Engineering, Dalian University of Technology, Dalian 116024, China

Received 8 June 2017; accepted 8 February 2018

Abstract: Two Fe–Al-based intermetallic aluminide coatings were fabricated on 430-SS (Fe–Cr) and 304-SS (Fe–Cr–Ni) substrates by pressure-assisted solid diffusion bonding with coating on pure Fe as control. The microstructure and intermetallic phases of the coatings were characterized by SEM, EDS and EBSD. A network of Cr₂Al₁₃ with matrix of Fe₄Al₁₃ was formed by inter-diffusing of Al with the substrates. The corrosion behavior of intermetallic coatings was investigated in 0.5 mol/L HCl solution by mass-loss, OCP, Tafel plot and EIS. It was found that corrosion resistance was greatly enhanced by dozens of times after the addition of Cr and Ni compared with that on pure Fe. The presence of cracks in the coating on 430-SS provided a pathway for corrosion media to penetrate to the substrate and accelerated the corrosion rate. Moreover, the corrosion product was analyzed by XRD, demonstrating that the addition of Cr and Ni facilitated the formation of more corrosion resistant phases, and therefore improved corrosion resistance.

Key words: intermetallic; iron aluminide; stainless steel; hydrogen chloride; corrosion

1 Introduction

The poor corrosion resistance of stainless steel in harsh environment, such as at high temperature, in aggressive chloride aqueous solution, requires strategy of applying additional protection [1–3]. Recently, the intermetallic aluminide coatings based on formation of adherent alumina layer have received extensive attention as their outstanding oxidation and corrosion resistance in aggressive chemical environments and even at temperatures as high as 1000 °C [4,5]. Thereinto, considerable interest arises on the research of intermetallic Fe–Al aluminide coatings due to much lower cost of raw materials, in comparison with intermetallic Ni–Al, Ti–Al, Nb–Al and Cu–Al aluminide coatings, which are being widely applied in industry [6,7].

There have been extensive efforts to produce intermetallic Fe-Al aluminide coatings by various

synthesis techniques [5,8–12]. Using laser surface alloying technique, different intermetallics of FeAl₃, Fe₂Al₅ and FeAl were successfully fabricated on low carbon steel [10]. Moreover, occurrence of a mixture of phases including Al-rich Fe₂Al₅, FeAl, Fe₃Al, and a Fe(Al) solid solution, varied significantly with Al content in the D-gun spraying process [11].

Furthermore, introducing alloying element or particles into the Fe–Al-based intermetallic aluminide coating is of great interest. The mechanical properties of Fe–Al–X composite coating can be highly improved by addition of B, Zr, Si and TiC particles [13–15]. Meanwhile, the incorporation of other noble elements, such as Ni and Mo, especially Cr, which are common elements in stainless steel, into the Fe–Al-based intermetallic aluminide coating is a potential consideration in the surface modification.

When dealing with bulk intermetallics, the strength can be improved over by 1000 MPa when FeAl contains solute additions (Cr, Mo), second phase or precipitates (Nb, Zr, C, B) [6]. Chromium addition as a ternary alloying element could reduce the sensitivity of binary Fe₃Al intermetallics to hydrogen embrittlement [16]. Moreover, adding small amount of Zr, Mo or Nb improved the oxidation kinetics of Fe₃Al–X in humid air at 950 °C. Fe₃Al showed massive spallation, whereas Fe₃Al–Zr, Fe₃Al–Zr–Mo and Fe₃Al–Zr–Mo–Nb produced a flat, adherent oxide layer [17]. Based on their excellent improvement on bulk intermetallics, it has motivated the incorporation of Cr, Ni or Mo into intermetallic aluminides of Fe–Al-based coating.

Moreover, the noble element incorporation has a significant advantage on the corrosion behavior of intermetallic aluminides of Fe-Al alloys or coating in aqueous solutions [18–21]. Cr as a ternary alloying element into the passive film on Fe₃Al substrate, had a tendency to enhance resistance to pitting corrosion and decrease the average density of pits in aqueous chloride solution [19]. The addition of Si or Ge modified the electrochemical response of Fe₃Al intermetallic aluminides, resulting in a more stable passive film, and improved resistance to the initiation of pitting corrosion in the presence of 100 mmol/L Cl⁻ [20]. It was also found that introducing Cr, Nb and Zr to Fe-28%Al alloy obviously enhanced the corrosion resistance in a low chlorinated medium [21]. However, aluminum-rich aluminides (Fe₄Al₁₃ and Fe₂Al₅) as the thermodynamic favored intermetallic phases in Fe–Al reaction system have not been studied on their corrosion behavior and limited literature data systematically compared corrosion of Al-rich aluminides coated on different iron-based substrates [22–24].

Here, we found a feasible way to incorporate Cr and Ni into the intermetallic aluminide coatings by easily diffusing from stainless steel substrate rather than by other alloying process, which will reduce cost of manufacture [25]. Two kinds of Fe-Al-based aluminide coatings were respectively fabricated by diffusion bonding pure aluminum on 430 (Fe-Cr) (430-SS) and 304 (Fe-Cr-Ni) (304-SS) stainless steel, in comparison with coating on pure Fe substrate. The alloying effects on microstructure, chemical composition, structure and the corrosion behavior of Al-rich Fe-Al aluminide coatings were investigated in 0.5 mol/L HCl solution. Additionally, the influence of Cr and Ni incorporation on the morphology and chemical composition of corrosion product was investigated.

2 Experimental

The commercial 1100 aluminum plates with different iron-based metal substrates (430-SS, 304-SS and pure Fe) were stacked as diffusion couples and placed in a clamp as shown in Fig. 1(a), and then put into

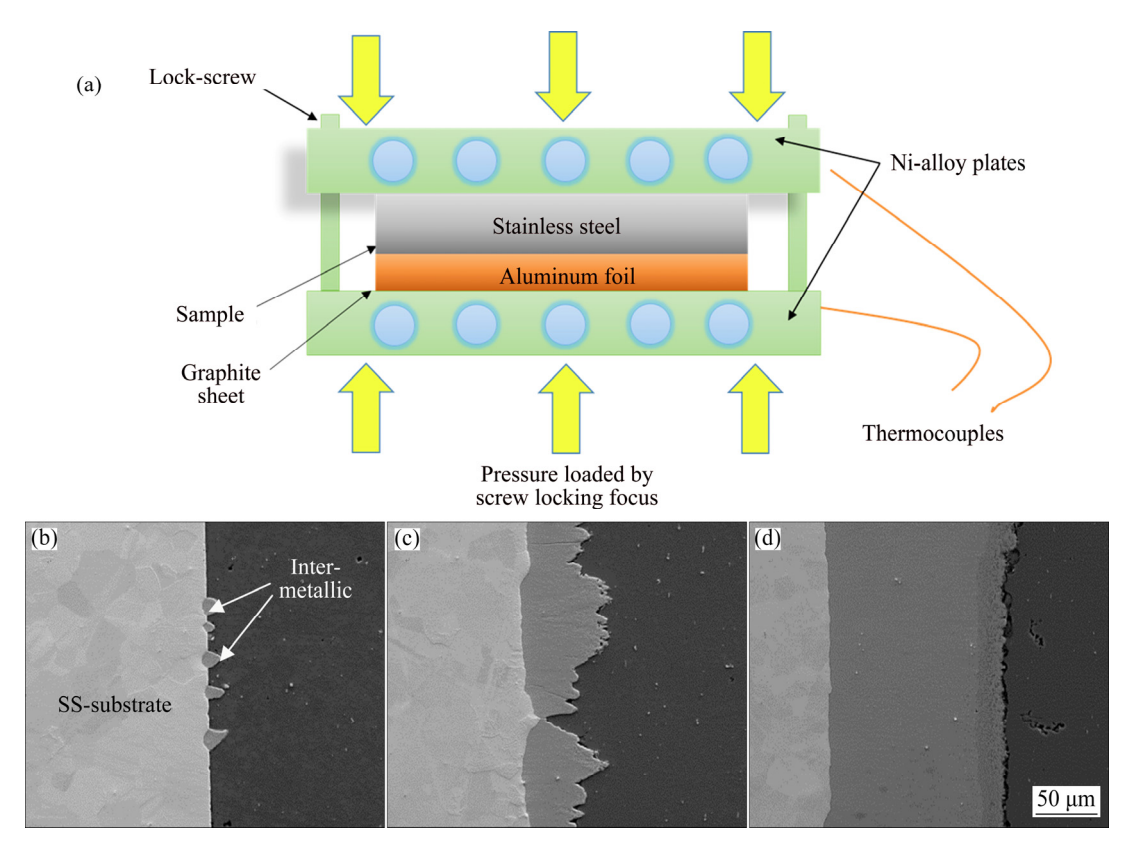


Fig. 1 Schematic diagram for fabrication of iron-based intermetallic aluminide coatings (a) and SEM images showing coating growth from formation of intermetallic nodules (b) to continuous coating (c, d)

the resistance furnace [23]. The composition of the iron alloy substrates is shown in Table 1. The dimensions of the samples processed for this work were 50 mm × 50 mm squares with 5 mm in thickness of Fe or SS substrate and 3 mm of aluminum. The solid diffusion bonding process was performed at 650 °C for 10 h and the pressure applied by the lock-screws of the clamp apparatus was 4 MPa. During the reaction, intermetallic nodules were firstly formed at the substrate and Al interface and then grew into continuous layer as shown in Figs. 1(b)–(d). After the reaction, the residual Al layer was removed by mechanical polishing to produce the formed intermetallic layer. The microstructure and phase formation analysis have been applied on both the cross direction and normal direction of the intermetallic layer.

Table 1 Chemical compositions of substrates 430-SS and 304-SS

Substrate	Molar fraction/%								
		Ni	Mo	Si	Mn	C	P and S	Fe	
430-SS	17.5	-	0.1	0.5	0.5	0.12	< 0.07	Bal.	
304-SS	18	8	0	0.5	0.8	0.06	< 0.06	Bal.	

Metallographic cross-sections with their finished surface oriented perpendicularly to the interface of the reacted layers were prepared by standard metallurgical grinding and polishing procedures. A Zeiss Supra 55 (VP) field emission SEM (Carl Zeiss AG, Jena, Germany) equipped with EBSD solid-state detector system was used to investigate the microstructure of the reaction layer and to measure the chemical composition and crystalline structure in selected areas.

The samples were cut into a rectangle with dimensions of 20 mm × 20 mm and treated as they received. Further surface treatment of the samples was not performed except washing with acetone for oil removal. The reason to keep the natural surface state was that in this work the materials were aimed to provide new options for application in industry without elaborate surface treatment. From another point of view, each surface finishing can reduce the coatings' thickness. Therefore, this study was limited to the untreated surface as a reference state in the following measurements.

The specimens for mass loss experiments were set in epoxy resin with a surface of 4 cm² and immersed in 100 mL of 0.5 mol/L HCl solution. The samples were weighed before and after 72 h immersion and mass losses were determined. Each measurement was performed on three separate intermetallic aluminide coating samples, and the average value was given. The corrosion rate was calculated by the following equation [26]:

$$v_{\rm d} = \frac{8.76(m_0 - m_1)}{\rho St} \tag{1}$$

where v_d is the corrosion rate (mm/a), ρ is the density of the coating (g/cm³), S is the surface area of specimens (m²), t is the immersion time (h), m_0 is the mass of specimen before immersion (g), and m_1 is the mass of specimen after immersion by removing corrosion product (g).

For electrochemical measurements, three-electrode configuration was used, with Ag/AgCl/3 mol/L KCl $(\varphi=0.210 \text{ V})$ as a reference electrode, Pt plate as a counter electrode, and intermetallic coating covered SS or pure Fe samples as the working electrode. The open circuit potential (OCP) curves of three kinds of coatings on 304-SS, 430-SS and pure Fe (304-Al coating, 430-Al coating, Fe-Al coating) in 0.5 mol/L HCl solution were monitored for 2000 s using CHI660D potentiostat controlled by a personal computer. Tafel plots were recorded from -1.0 to 0.2 V with a scanning rate of 0.5 mV/s in 0.5 mol/L HCl solution. EIS measurements were conducted in the frequency range from 100 kHz to 10 mHz at the OCP with a potential perturbation of ±10 mV, which were performed with a CHI660D potentiostat. All the potentials are referred to Ag/AgCl/ 3 mol/L KCl electrode.

The distribution of corrosion product and corrosion morphology was observed by EDS and SEM. Moreover, the corrosion product of the specimens was investigated with X-ray diffractometry (XRD) manufactured by Rigaku using Cu K_{α} radiation.

3 Results and discussion

3.1 Microstructure characterization

The intermetallic coatings fabricated on 430-SS, 304-SS and pure Fe were observed by SEM and EDS. As shown in Fig. 2, the diffusion of Cr and Ni from the substrate results in great variation on the roughness of intermetallic coatings. A coarse intermetallic coating with higher porosity was formed on pure Fe substrate. In comparison, a relatively smooth coating was attained on 430-SS with some small pores and cracks shown in Figs. 2(b₂) and (b₃); while, the addition of both Cr and Ni leads to a dense and smooth coating formed on 304-SS substrate. As shown in Figs. 2(b₃) and (c₃), the pore density of coating on 304-SS is greatly declined as compared with that on 430-SS substrate. demonstrated by EDS analysis, Cr or Cr and Ni elements are successfully introduced to the coating surface in the solid diffusion process. With regard to coating on 430-SS, Cr is partly concentrated in certain regions with Fe and Al elements uniformly distributed. After extra addition of Ni, all the elements distributed more evenly in intermetallic coating on 304-SS substrate.

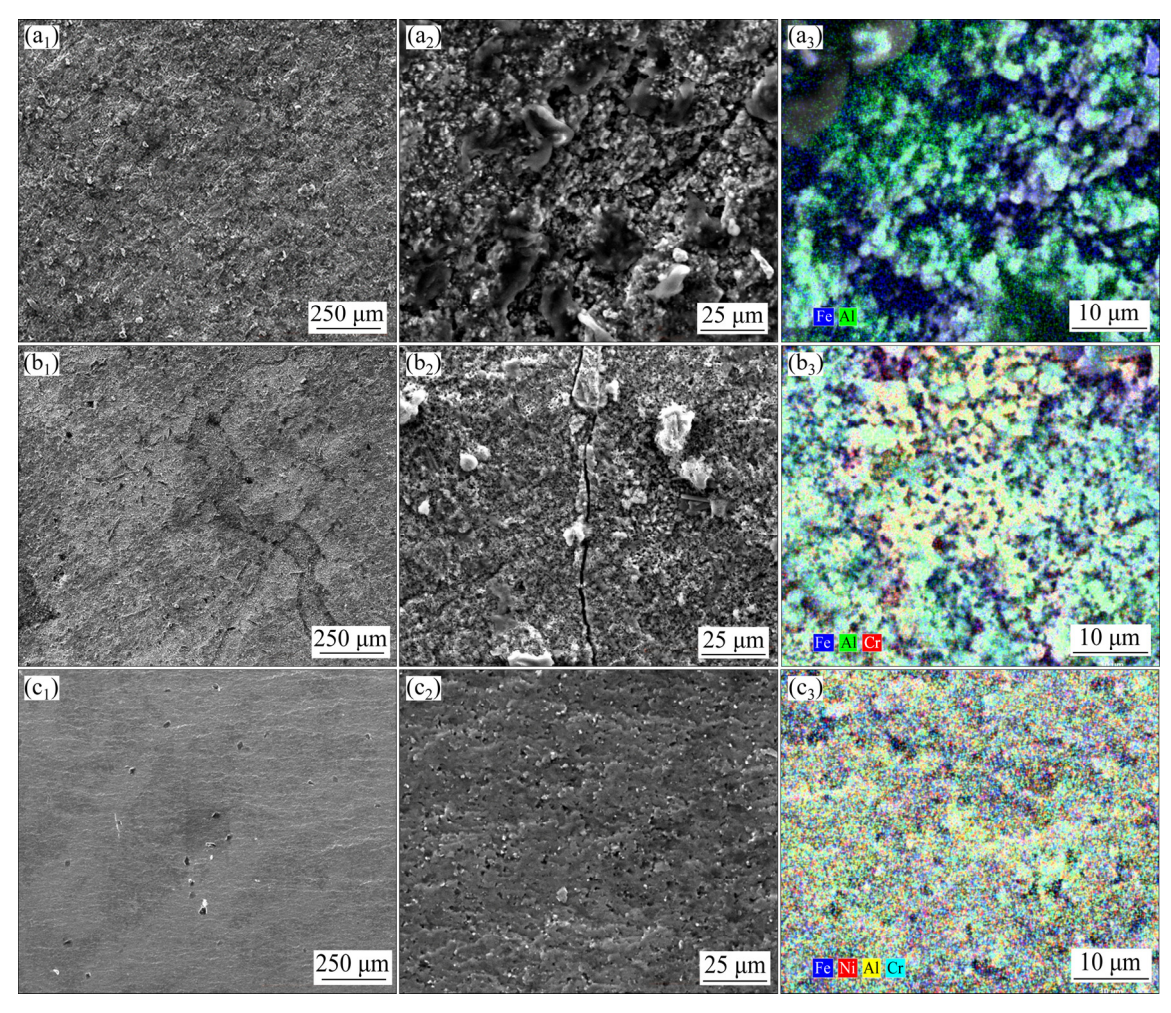


Fig. 2 Top views (a_1-c_1, a_2-c_2) and EDS mapping (a_3-c_3) of intermetallic layers formed on pure Fe (a_1-a_3) , 430-SS (b_1-b_3) and 304-SS (c_1-c_3) (Symbol of colors: dark blue (Fe) and green (Al) in (a_3) ; dark blue (Fe), green (Al) and red (Cr) in (b_3) ; dark blue (Fe), yellow (Al), red (Ni) and light blue (Cr) in (c_3))

The cross-section of intermetallic layer was further elucidated. Figure 3 shows that the intermetallic surface coating is compact and dense on 304-SS substrate, compared with several small cracks presented on 430-SS substrate and a tongue-like structure on pure Fe; whereas, all the intermetallic coatings grow intact on the substrates. Moreover, different intermetallic aluminide phases are formed due to incorporation of chrome and nickel elements by adjusting the composition of substrate.

Figure 4 shows the chemical composition profiles across the intermetallic coatings of the three substrates. The elemental distribution in each intermetallic coating highly corresponds to their microstructures. Figure 4(a) shows only one intermetallic layer with about 28% Fe (molar fraction) formed on pure Fe substrate which confirmed that the intermetallic phase is Fe₂Al₅ according to the molar ratio of Fe to Al close to 1:2.5 and our previous study [27,28]. While, the addition of Cr or both Cr and Ni into the Fe–Al aluminides coating have

generated a multi-layer structure presented in the 430-SS and 304-SS intermetallic coatings.

The intermetallic coatings on the 430-SS and 304-SS substrates (shown in Figs. 4(b) and (c)) are mainly composed of a uniform layer with 70%Al-25%Fe-5%Cr (molar fraction). These molar fractions of Fe, Cr and Al elements are corresponding to the Fe₂Al₅ phase region in the Al-Fe-Cr ternary phase diagram and confirmed in our previous study [28,29]. Hence, the main intermetallic phases formed in the 430-SS and 304-SS substrates are Fe₂Al₅ phase with Cr or Cr, Ni as solid solution. However, the addition of Cr and Ni elements has led to an Al-rich intermetallic layer formed in the front of the coating layer. The corresponding elements distribution in the Al-rich layer is shown in Fig. 3(d) where the Cr-rich phase is in the matrix of iron-rich phase with a two-phase co-exited feature. This layer is named as two-phase layer. Additionally, a precipitation layer with lots of Cr-rich particles precipitating on the iron-based matrix forms adjacent to the two-phase layer

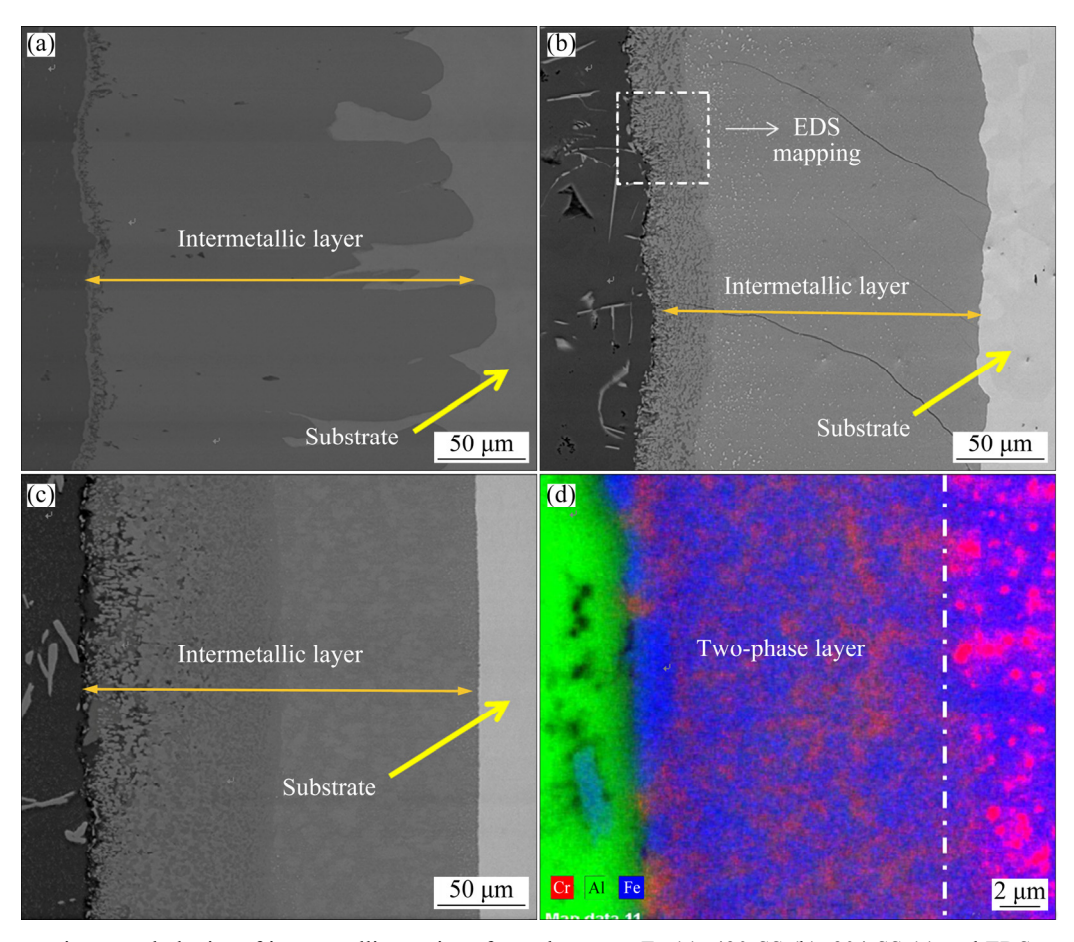


Fig. 3 Cross-section morphologies of intermetallic coatings formed on pure Fe (a), 430-SS (b), 304-SS (c) and EDS mapping result of two-phase layer in coating on 430-SS (d)

as shown in Figs. 3(d) and 4(b). In order to more clearly identify the intermetallic phases formed in the two-phase layer, further crystallographic information was obtained by EBSD phase mapping along with the diffraction pattern of the selected phases, as shown in Fig. 5. The representative indexed diffraction patterns from the two-phase layer shown in Figs. 5(b) and (c) reveal that the crystallographic structures of the iron-rich phase is monoclinic Fe₄Al₁₃ (space group C2/m, a=1.5489 nm, b=0.8083 nm and c=1.2476 nm, c/a=107.72) and the Cr-rich phase (green) is Cr₂Al₁₃ phase (space group C/2m, a=2.5196 nm, b=0.7574 nm and c=1.0949 nm, c/a=128.71). Based on interaction between pure aluminum and Fe-Cr stainless steel, this two-phase co-exiting feature was formed partly by the solid state diffusion and partly by the solidification of the locally melted pure Al [25]. The EBSD phase mapping result also confirms the main intermetallic phase as Fe₂Al₅ (space group Cmcm, a=0.7649 nm, b=0.6413 nm and c=0.4216 nm, shown in red Fig. 5(a). Cr diffusing into the coating layer also introduces some of Cr-containing precipitates Al₄Cr (yellow area in Fig. 5(a), space group P_6mnm , a=1.74 nm, c=4.41 nm) formed in the uniform layer as fluctuation of Cr concentration on the right side of the composition profile of uniform layer in Fig. 4(b).

Moreover, since additional 8% Ni in 304-SS, there are still some nickel-containing nodules formed in the uniform layer as fluctuation of Ni and Fe elements distributed in the uniform layer (Fig. 4(c)). These Ni-rich particles were also identified in the reaction layer while 306-SS was reacted with semi-solid Al, forming Fe_0 7 Ni_1 3 Al_9 phase in the Fe_2Al_5 matrix [29]. Fe_0 7 Ni_1 3 Al_9 phase was also designed as Fe_rNi_{1-r}Al₉ phase and reported with the lowest thermodynamic formation energy in Al-Fe-Ni system [27,30]. The formation of this phase caused the absence of Cr-rich precipitate layer in the 304 substrate as compared with Figs. 4(b) and (c). Another change caused by the addition of Ni expands the proportion of two-phase layer in the total reaction layer of 304-SS sample compared to the 430-SS sample. According to the Al-Fe-Ni [31] and Al-Cr-Ni [32] ternary phase diagrams, the addition of Ni will decrease the solubility of Fe and Cr in Al and move the eutectic point towards the Al side, which would benefit the Fe-Al and Al-Cr eutectic reaction and lead to faster growth of the Cr-containing phases in the two-phase layer. Therefore, the addition of Ni was beneficial to the formation of two-phase layer.

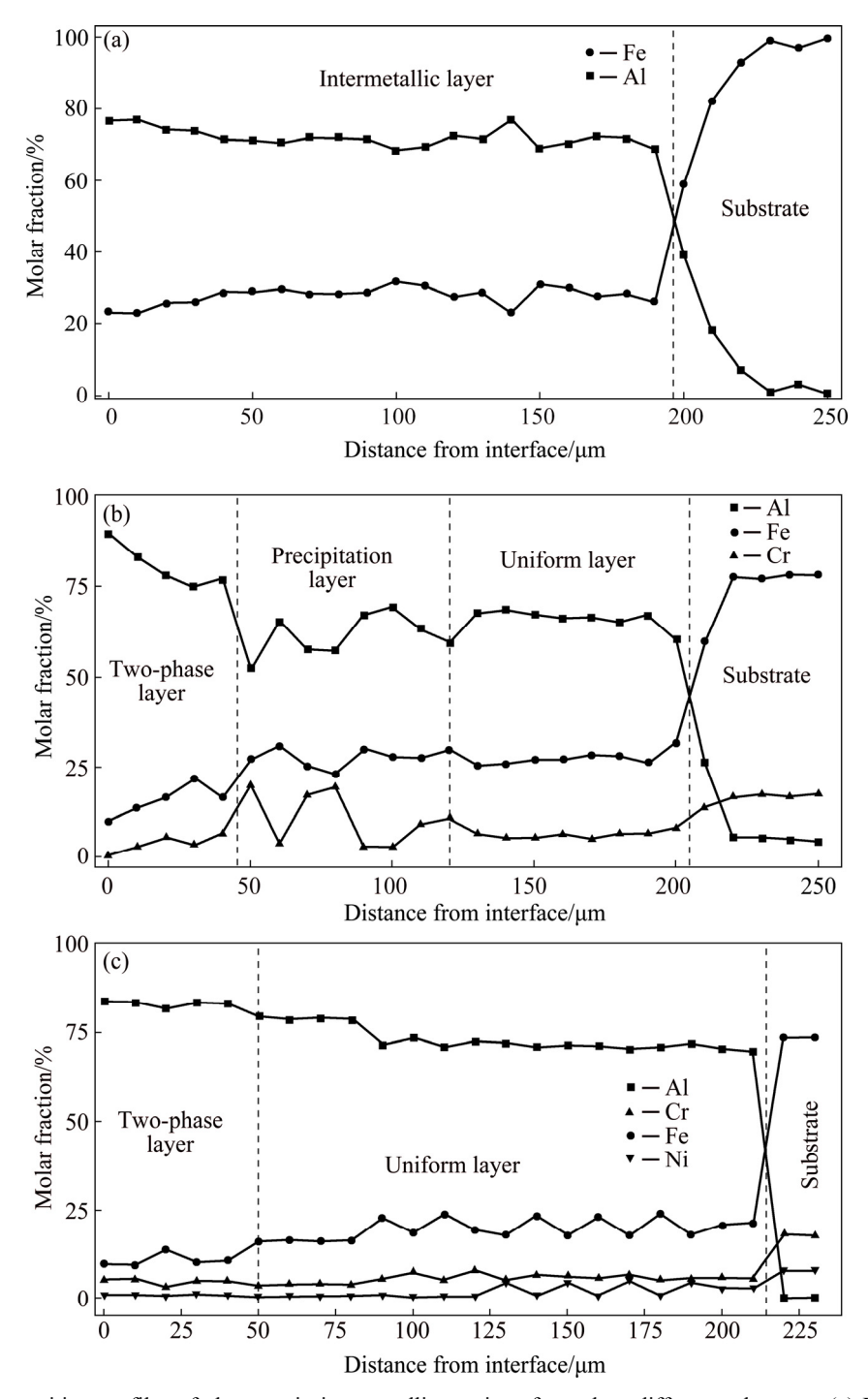


Fig. 4 Chemical composition profiles of elements in intermetallic coatings formed on different substrates: (a) Pure Fe; (b) 430-SS; (c) 304-SS

3.2 Mass loss test and electrochemical measurements

Figure 6 shows the corrosion rates calculated from the mass loss test after immersion in 0.5 mol/L HCl solution for 72 h. Clearly, the corrosion rate of intermetallic aluminide coating on Fe substrate is the maximum among the three coatings, around 35 mm/a. After the addition of Cr, the corrosion rate is 19 mm/a, less than half decrease when compared with that on Fe–Al coating. The addition of both Cr and Ni realizes

an obvious decline of corrosion rate. Around 1.1 mm/a is observed on 304-Al coating, confirming their great benefit on the corrosion resistance of intermetallic aluminide coatings.

Moreover, three intermetallic aluminides of Fe–Al-based coatings were evaluated by open circuit potential measurement. As shown in Fig. 7, when intermetallic aluminide coatings are immersed in 0.5 mol/L HCl solutions there is no obvious OCP

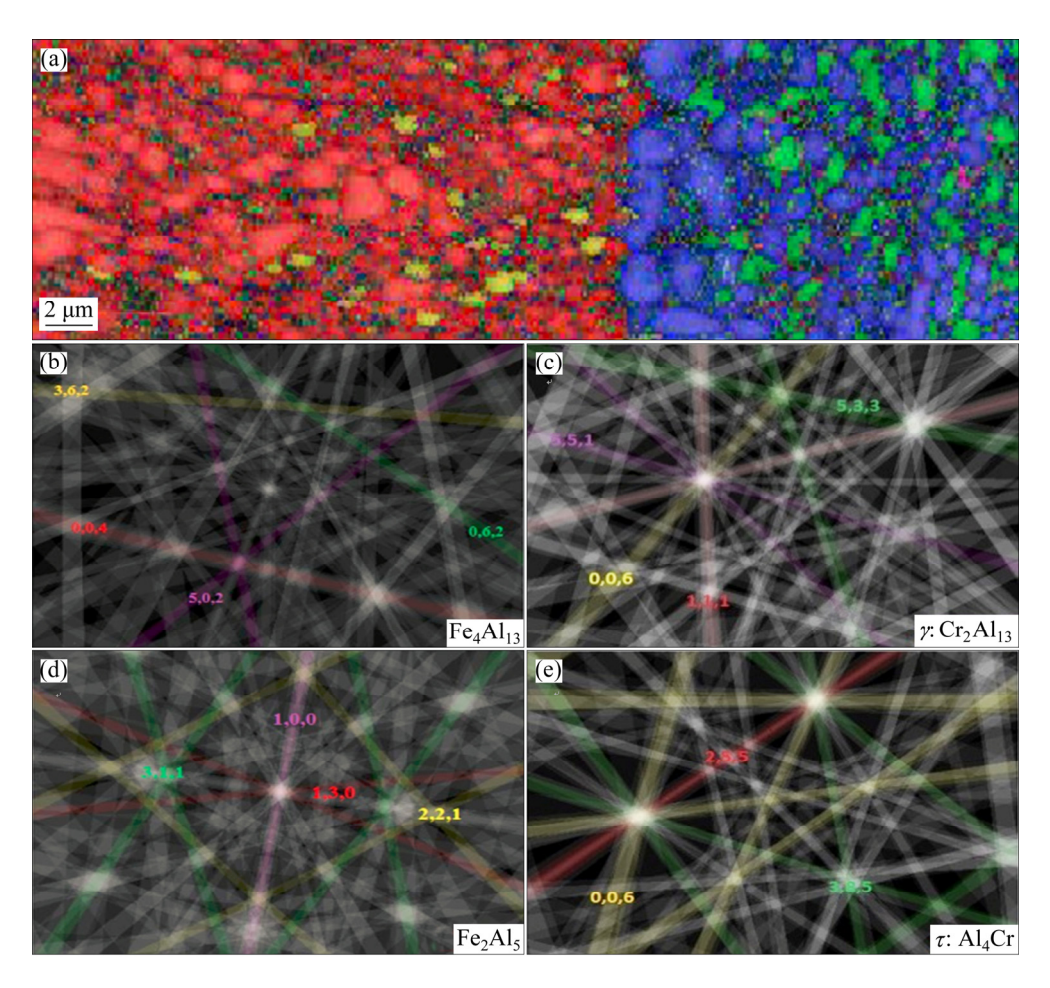


Fig. 5 Color-coded EBSD phase map for 430-SS/Al reaction (in two-phase layer: Fe_4Al_{13} phases are blue; Cr_2Al_{13} phases are green; in uniform layer: Fe_2Al_5 phases are red; Al_4Cr phases are yellow) (a) and representative indexed diffraction patterns (b–e) by EBSD spot mode: (b) Fe_4Al_{13} ; (c) Cr_2Al_{13} ; (d) Fe_2Al_5 ; (e) Al_4Cr

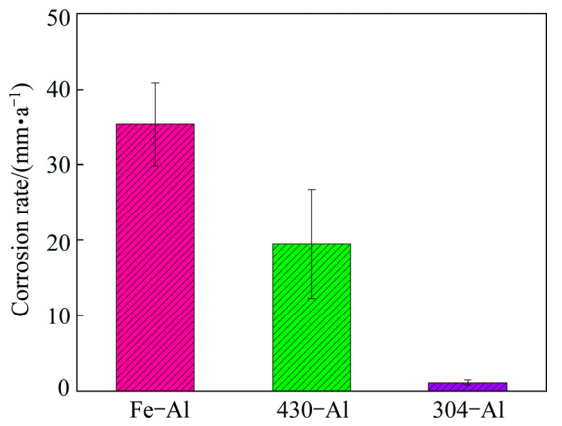


Fig. 6 Corrosion rate obtained by mass loss test in 0.5 mol/L HCl solution

fluctuation that corresponds to the breakdown and re-passivation of surface layer, ascribing to the rapid dissolution of the surface layer in strong acidic solution. The OCP of intermetallic aluminide coatings on pure Fe is gradually declined from -0.65 to -0.68 V during the initial 800 s immersion, then keeps stable in the following 800 s, and eventually shows a slight increase

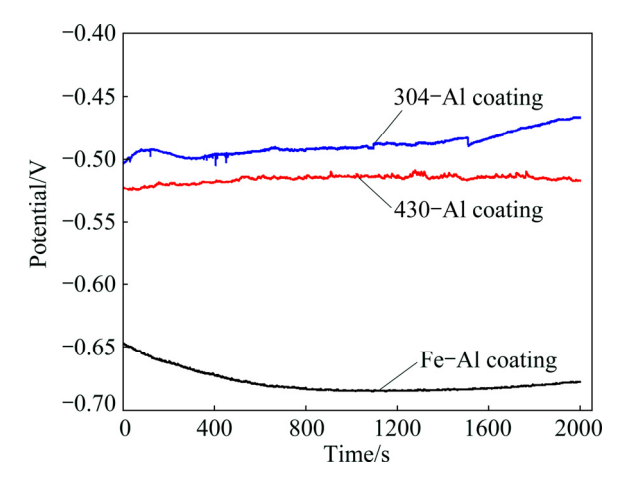


Fig. 7 Evolution of open circuit potentials of intermetallic coatings formed on 430-SS, 304-SS and pure Fe with time in 0.5 mol/L HCl solution

in the last 400 s immersion. Introducing Cr or both Cr and Ni elements, OCPs of aluminide coatings on 430-SS and 304-SS are significantly shifted to more noble values. It is noted that the OCP of aluminide coatings on 430-SS is more stable in comparison with that on 304-SS, with a

relatively constant value of around -0.52 V, which is related to the enrichment of Cr element on the surface coating as confirmed by the EDS mapping result in Fig. 2. It is known that Cr-doped intermetallics have the tendency to broaden the passivation and reduce the sensitivity of alloys to pitting corrosion in Accordingly, Cl⁻-containing solution [19,21]. the introduction of Cr in our work facilitates re-passivation of surface coating on 430-SS substrate. Consequently, the chemical dissolution and breakdown of the surface coating are greatly inhibited in the short time attack of HCl solution, therefore enhancing their corrosion resistances. Furthermore, extra addition of Ni element on the aluminide coatings on 304-SS substrate results in much more positive shift of OCP to -0.48 V at the start of immersion, following a constantly slow increase of OCP until reaching -0.46 V. In this regard, the incorporation of Ni into the surface coating and the presence of intermetallic phases Cr₂Al₁₃ and Fe_{0.7}Ni_{1.3}Al₉ explained the noblest value of OCP on coating of 304-SS. in accordance with the literature in which intermetallic Ni-Al aluminides exhibit better oxidation and corrosion resistance than Fe-Al aluminides [6]. The slight increase of OCP in the following immersion should be ascribed to the formation of passive network of Cr₂Al₁₃ in the two-phase layer as shown in Fig. 3.

Tafel polarization tests were also conducted. As shown in Fig. 8, the intermetallic aluminide coatings on 304-SS and 430-SS substrates exhibit similar electrochemical behaviors with regard to that occurring on pure Fe. Instead of active-passive behavior usually represented for intermetallic Fe-Al aluminides in the chloride-containing circumstances [18–21,33], activation behavior controlled by electrochemical polarization is dominated in cathodic and anodic processes, respectively 2H⁺+2e=H₂↑ and Fe-2e=Fe²⁺, Al-3e=Al³⁺ accompanied by the dissolution of trace elements such as Ni and Cr, which should be ascribed to the strong acidic media and more concentrated chloride ions. It is known that the iron aluminides have high susceptibility to corrosion pitting in media with contents of Cl⁻ [34], and an obvious passive platform is shown in anodic branch of Tafel plots. The phenomenon of pitting corrosion was also displayed in the intermetallic Fe-Al aluminides [19,21]. The minimum concentration of 6×10⁻⁴ mol/L Cl⁻ was required to break down the passive layer and to cause pitting corrosion [35]. With the increase of the chloride ion concentration, the passive range was narrowed and the repassivation of the intermetallics after transpassive potential was prevented even after addition of Cr [19,22]. On the other hand, the acidic media would facilitate the chemical dissolution of passive layer on intermetallic Fe-Al aluminides, demonstrating a narrowed passive range, or more than that, its inexistence in the anodic

branch of Tafel plots [19,36]. Therefore, the much higher concentration of chloride ions and more acidic circumstance in our work resulted in the disappearance of passive range. As deduced from Tafel plot (shown in Table 2), the corrosion potentials are shifted to more noble values after the introduction of Cr or both Cr and Ni, from -0.46 V for coating on 430-SS to -0.42 V for coating on 304-SS, in comparison with -0.67 V on pure Fe. It is not very impressive that the corrosion current density decreases from 8.89, 6.49 to 3.83 mA/cm² after introduction of Cr or both Cr and Ni, relating to the strong chemical dissolution of surface layer in acidic media. As performed strong polarization in Tafel plot measurement, the corrosion current density could not represent the actual corrosion rate.

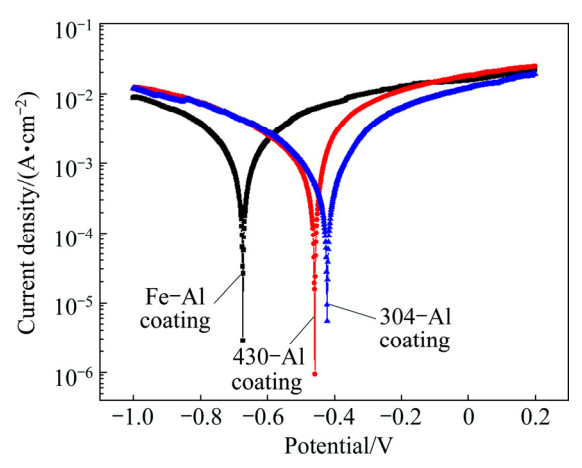


Fig. 8 Tafel curves of intermetallic coatings formed on 430-SS, 304-SS and pure Fe in 0.5 mol/L HCl solution

Table 2 Electrochemical parameters obtained from polarization curves

Coating	$\varphi_{\rm corr}({\rm vs\ Ag/AgCl})/{ m V}$	$J_{ m corr}/({ m mA\cdot cm}^{-2})$
Fe-Al	-0.67	8.89
430-A1	-0.46	6.49
304-A1	-0.42	3.83

As a non-destructive method, EIS was applied to investigating the corrosion behavior of intermetallic aluminides of Fe-Al-based coatings in 0.5 mol/L HCl solution. After stabilization of free corrosion potential in 5 min, Bode and Nyquist plots were recorded as shown in Fig. 9. For all coatings, Bode plots Fig. 9(a) show at least two time constants as the presence of widened phase angles at high frequencies (HFs) and medium frequencies (MFs). Accordingly, Nyquist spectra exhibit two overlapped capacitive loops at HFs and MFs in Fig. 9(b), although those two capacitive loops are not easily distinguished from each other. At low frequencies (LFs), an arc or tail in the Nyquist plots is demonstrated as inductive behavior or diffusion behavior. Additionally,

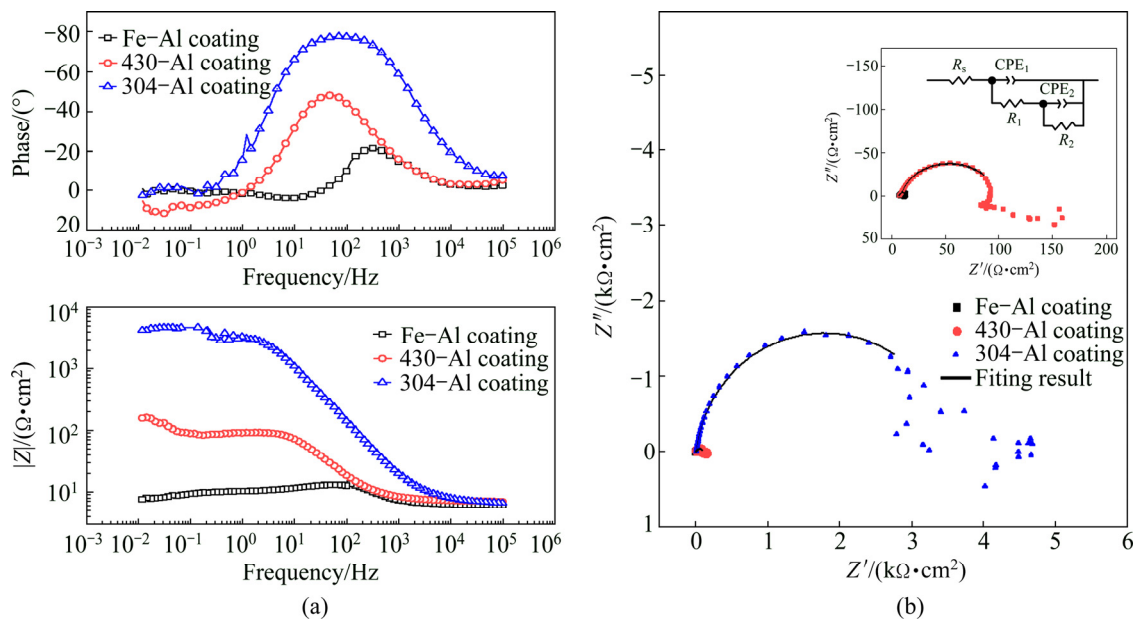


Fig. 9 Bode (a) and Nyquist (b) plots of intermetallic coatings formed on pure Fe, 430-SS and 304-SS in 0.5 mol/L HCl solution and their corresponding equivalent circuit model

the existence of an inhomogeneous electrode surface could be seen in the EIS measurement, where the phase angle minima are less than 90°, which was in accordance with the coarse surface state of coatings in Fig. 2 [35]. It is apparent that the minima of phase angle are related to the roughness of the coatings. With the increase of the roughness and porosity, the minima of phase angle are inclined to smaller values, consisted with research in Ref. [37]. Furthermore, the *Z* module values decrease in the following order of 304–A1, 430–A1 and Fe–A1 coating, verifying that the introduction of Cr or both Cr and Ni greatly enhanced the corrosion resistance of coatings in short time attack of HCl solution.

Due to the dissolution of passive coating caused by strong acidic HCl solution and their high porosity, Nyquist and Bode plots exhibited differently with those in the low concentration of chloride ions circumstance which is correlated to the compact passive layers on the intermetallic aluminides with minor attack of chloride ions, for example, in 0.001 mol/L NaCl solutions or 0.1 mol/L Cl addition to buffer solution with pH 8.4 [19,20,38]. As shown in Fig. 9(b), the capacitive loop at HF is related to the performance of the surface films (including corrosion product film), while the diameter of MF capacitive arc is associated with the charge-transfer resistance, subsequently, with the corrosion resistance. The diffusion or inductive behavior at low frequencies (LFs) is not further discussed in our work. The existence of diffusion tail is probably ascribed to the difficulty in the diffusion of charged electrolyte across the surface film to the substrates. While, the inductive arc may attribute to relaxation processes involving the dissolution of metal to ion, leading to the formation of corrosion product and the adsorption of electrolyte-active species at localized defective sites [38].

Here, an equivalent circuit with two time constants in Fig. 9(b) was presented to fit the EIS results, where R_s is the solution resistance, R_1 is the resistance of the surface film, R₂ is charge-transfer resistance, CPE₁ represents constant phase elements of the surface film, and CPE₂ is constant phase elements of the electric double layer. As shown in Fig. 9(b), the equivalent circuit fits the experimental results very well, indicating that the equivalent circuit is suitable and reasonable. The fitting results are shown in Table 3. It is obvious that the corrosion resistance of (R_1+R_2) is greatly enhanced by 300 folds after addition of both Cr and Ni in short time immersion. While around 10 times improvement on corrosion resistance is realized after introducing single Cr element when compared with that on coating of pure Fe.

Overall, the analysis above clarifies the beneficial effect of Cr or both Cr and Ni addition on the corrosion resistance of intermetallic aluminides of Fe–Al-based coating, revealing that multiple introduction of Cr and Ni facilitates the formation of much denser and more compact surface coating, thereby improving the corrosion resistance around dozens of times by extra Ni addition, better than single addition of Cr.

3.3 Corrosion morphology and corrosion product

The corrosion morphology in long term corrosion test in 0.5 mol/L HCl solution was investigated by SEM without post-processing for corrosion product removal.

Table 3 Fitting results obtained from equivalent circuit for three intermetallic coatings on Fe, 430-SS and 304-SS in 0.5 mol/L HCl solution

Coating	$R_{\rm s}/(\Omega\cdot{\rm cm}^2)$	CPE_1 - $T/(F \cdot cm^{-2})$	CPE ₁ -P	$R_1/(\Omega \cdot \text{cm}^2)$	CPE_2 - $T/(F \cdot cm^{-2})$	CPE ₂ -P	$R_2/(\Omega \cdot \text{cm}^2)$	$(R_1+R_2)/(\Omega\cdot\mathrm{cm}^2)$
Fe-Al	5.8	4.9×10^{-5}	0.83	1.2	1.7×10^{-4}	0.88	9.5	10.7
430-A1	7.1	1.9×10^{-4}	0.85	10.9	7.3×10^{-5}	0.92	82.5	93.4
304-A1	6.5	7.6×10^{-6}	0.94	6.9	1.1×10^{-5}	0.91	3552	3558.9

 R_s is the solution resistance; R_1 is the resistance of the surface film; R_2 is charge-transfer resistance; CPE_1 -T and CPE_2 -T are the values of constant phase elements of the surface film and the electric double layer, respectively; CPE_1 -P and CPE_2 -P are dimensionless ratios of CPE_1 and CPE_2 to pure capacitance, respectively; R_1+R_2 is the sum of the resistance

Due to the strong acidic circumstances (pH 0.3) and high solubility of the precipitates in acid, no apparent corrosion product is visible in Fig. 10. All of the three coatings display uniform corrosion after 72 h immersion in acidic solution. There is no doubt that the coating on pure Fe is terribly corroded with regard to coatings on 430-SS and 304-SS and a honeycomb-like structure is formed after 72 h attack. Obviously, Fe element dominates in EDS result with little Al and O elements, predicating that the intermetallic coating on pure Fe would probably be totally corroded and provide no more protection after 72 h immersion. In comparison, the coating on 304-SS is relatively dense with Al, Ni and Cr enrichment on the surface, forming a compact structure to inhibit further corrosion. Nevertheless, corrosion on coatings of 430-SS substrate is dominated by the cracks formed during the fabrication. Compared with Fig. 2, much deeper and wider cracks appear on the top view of the surface coating, regardless of Cr incorporation. Preferential corrosion attack on intermetallic coating of 430-SS should be initiated from the cracks and go deeper inside as the acidic electrolyte penetrates into and finally reaches the substrate. It is indicated that the introduction of Cr to coating on 430-SS is somewhat protective on the premise of absence of cracks. Better protection is provided after addition of both Cr and Ni elements. A much denser and more compact structure of the coating on 304-SS contributes to the long-term corrosion resistance.

Furthermore, the corrosion morphologies of cross sections and their corresponding EDS of three intermetallic coatings are shown in Fig. 11. It is clear to see that the intermetallic coating on pure Fe, which is around 200 µm in thickness (as shown in Fig. 4), is almost corroded and small tongue-like structures stand on the substrate with thickness around several tens of micrometers. In accordance with Fig. 10, many cracks appear on the coating of 430-SS substrate, providing pathways for the electrolyte to reach the substrate. Thereafter, galvanic corrosion can be observed at the interface of coating and substrate, the coating is dissolved as an anode coupling with 430-SS as a cathode which may result in the peeling of the coating. After addition of both Cr and Ni, the intermetallic coating on 304-SS is complete and compact. Two intermetallic

layers remain clear to see, with dark grey two-phase layer and light grey uniform layer. The two-phase layer with high concentration of Al (more than 80%) is more resistant in strong acidic media. According to Figs. 3 and 4, two-phase layer with intermetallic phases of Fe₄Al₁₃ and Cr₂Al₁₃ is formed during fabrication. Fe₄Al₁₃ phase is preferentially corroded by strong acidic media and Cr₂Al₁₃ phase remains stable and builds a network structure during the long term corrosion, which is confirmed in Fig. 10. Apart from the cracks shown in Figs. $10(b_1)$ and $11(b_1)$, the corrosion morphology and EDS result on coatings of 430-SS are similar to those on coating of 304-SS substrates, which is attributed to similar structure of intermetallic layer with presence of both Fe₄Al₁₃ and Cr₂Al₁₃ phases. However, the proportion of two-phase layer in the total reaction layer of 304-SS sample is greater compared with the 430-SS sample. These indicate that the addition of Ni is beneficial to the formation of two-phase layer, thereby enhancing the corrosion resistance of the coatings.

Moreover, the corrosion product on the coating surface was investigated by XRD, and the results are shown in Fig. 12. Due to the complete dissolution of intermetallic coating on pure Fe, most peaks are related to the pure Fe substrate, in agreement with the corrosion morphologies and EDS results in Figs. 10 and 11. In addition, there are several peaks corresponding to Fe₂Al₅ phases, since some small tongue-like structures remained on the coating surface after 72 h immersion. In regard to the intermetallic coatings on 430-SS, there exist peaks corresponding to the Al_{58.5}Fe_{3.2}Cr_{10.3} phase besides peaks related to Fe₂Al₅ phase and Fe substrate. It is elucidated that the presence of more corrosion resistant phase of Al_{58 5}Fe_{3 2}Cr_{10 3} should contribute to the enhanced corrosion resistance of intermetallic coatings on 430-SS. Furthermore, both Fe₄Al₁₃ and Cr₂Al₁₃ phases, which are dominated in the top layer of coating in the microstructure analysis (Figs. 3 and 4), were detected on coating of 304-SS in XRD pattern, demonstrating that the addition of Cr and Ni facilitates a compact coating layer on 304-SS and greatly inhibits the corrosion attack from the acid.

3.4 Corrosion model

It is well known that Cr and Al elements are

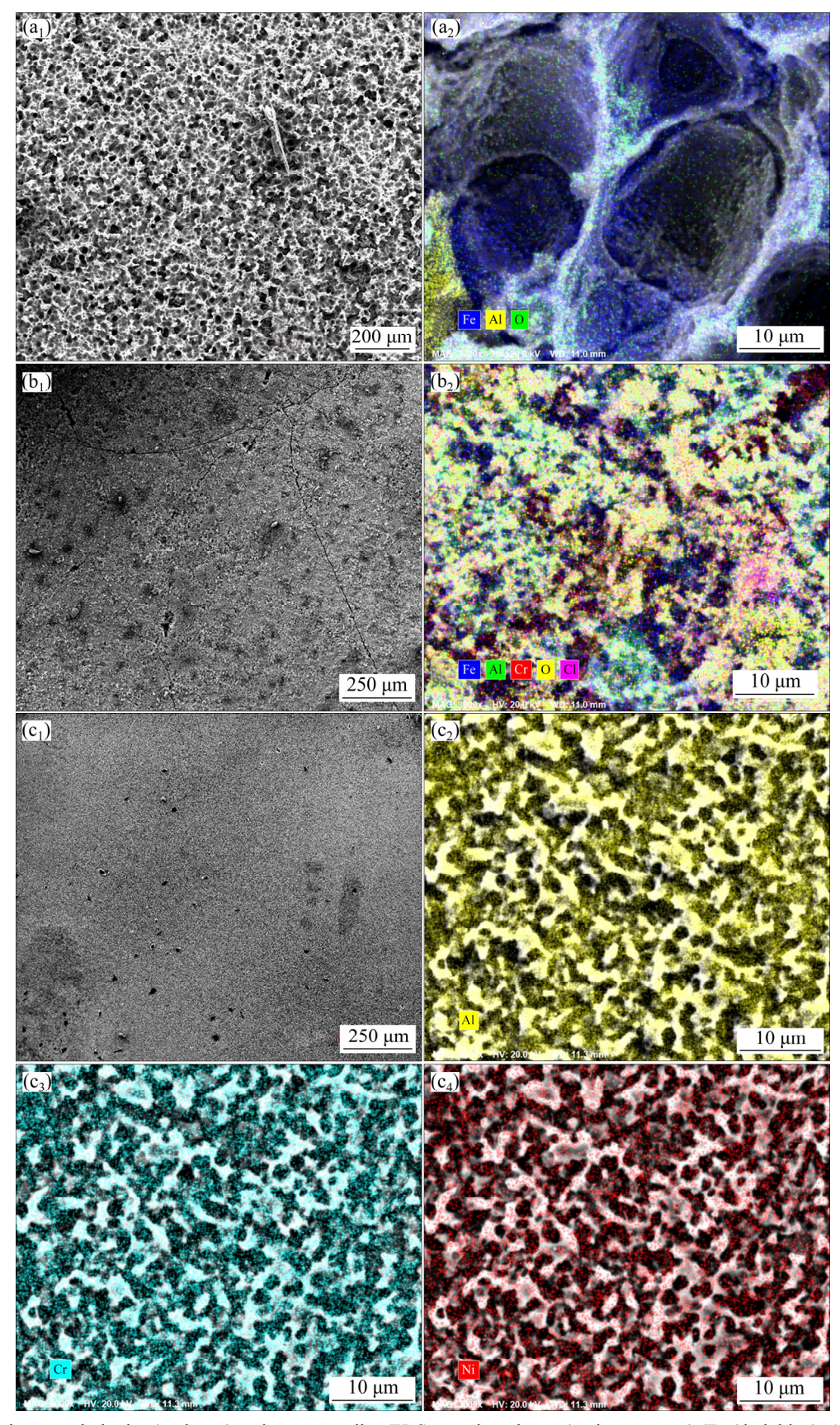


Fig. 10 Corrosion morphologies (a_1, b_1, c_1) and corresponding EDS mapping photos $(a_2, b_2, c_2, c_3, c_4)$ (Fe (dark blue), Al (yellow) and O (green) distributions in (a_2) ; Fe (dark blue), Al (green), Cr (red) and O (yellow) in (b_2) ; Al (yellow) distribution in (c_2) ; Cr (light blue) distribution in (c_3) and Ni (red) distribution in (c_4) of intermetallic coatings on pure Fe (a_1, a_2) , 430-SS (b_1, b_2) and 304-SS (c_1-c_4) after 72 h immersion in 0.5 mol/L HCl solutions

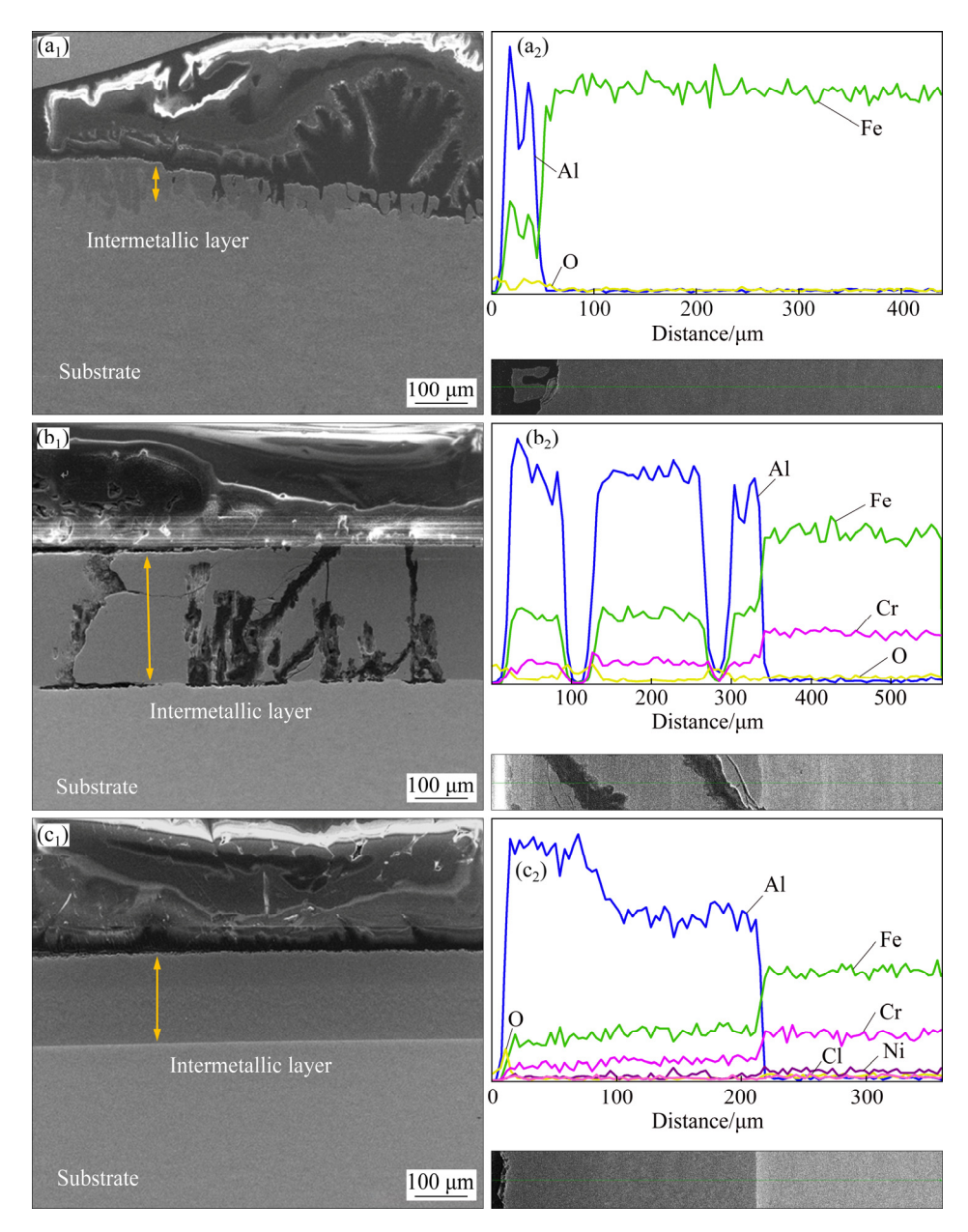


Fig. 11 Corrosion morphologies of cross sections (a_1-c_1) and their corresponding EDS line mapping results (a_2-c_2) of intermetallic coating on pure Fe (a_1, a_2) , 430-SS (b_1, b_2) and 304-SS (c_1, c_2)

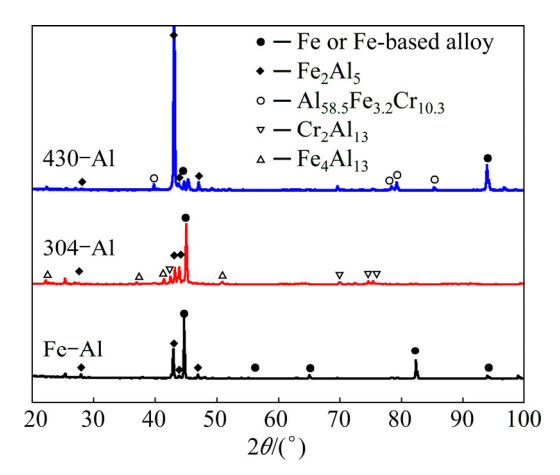


Fig. 12 XRD patterns of intermetallic aluminide coatings on three different substrates

significant in the surface modification. As noticed, Cr which is an important element in the stainless steel or as a predominated candidate in the Fe-Cr or Fe-Cr-X (X=Ni, Ru, Co) alloys, usually induces passivity in Fe-based alloys [39-44]. An apparent active-passive transition is dominated in anodic polarization measurements in stainless steel and Fe-Cr-based alloys, which is attributed to the formation of a passive film [40,42,43]. Various researches have verified that the passive film is mainly composed of Cr(OH)₃ and Cr₂O₃ in the acidic solutions free of chloride ions [39,40,42,44]. Chloride ions, to some extent, have deteriorated the passivity of surface film in stainless steel and Fe-Cr-based alloys and enhanced their sensitivity to pitting corrosion [40,42,44].

The addition of Al is also of importance as Al is likely to form a protective film in aqueous solution [45]. Of which, Al-based complex metallic alloys (CMAs) are found to be highly corrosion resistant in strong acid and alkaline solutions [46-50]. BARTHÉS-LABROUSSE et al [49] performed a detailed research on Al-Cr-Fe complex metallic alloy, of which the chemical composition is similar to our two-phase layer. The formation of a AlO(OH) richer surface induces a passivation effect but is detrimental because of the higher susceptibility to localized attack in the more aggressive environment of 0.01 mol/L HCl. Other researches also verified that Al-Cr-Fe CMAs exhibit passive stability in extreme pH solutions as the enrichment of the outermost Al (hydr)-oxide layer by Cr³⁺ oxide, but there is no doubt that the aggressive chloride ions induce pitting corrosion attack [46].

In the present work, two intermetallic aluminide coatings on 430-SS and 304-SS were fabricated. As shown in Figs. 2-5, an Al-rich intermetallic layer with two-phase co-exited feature formed at the front of the coating layer on 430-SS and 304-SS. It is confirmed by EDS and EBSD that the two-phase layer consists of Cr₂Al₁₃ phase dispersed in the matrix of Fe₄Al₁₃. As discussed above, the addition of Cr would passivate the surface film and enhance the corrosion resistance in the acidic solution [39-44]. On the other hand, a similar chemical composition of two-phase layer with Al-Cr-Fe CMAs, provides essential protection from chloride ion attack in the acidic solution. As demonstrated in Fig. 7, the open circuit potentials of 304-Al and 430-Al coatings shifted to positive values compared with Fe-Al coating. Mass loss test in Fig. 6 and EIS results in Fig. 9 show great corrosion resistance enhancement is realized on 304-Al coatings. It is apparent that Al coating containing Cr or Cr and Ni plays a vital role in the corrosion inhibition of acidic solution attack. As shown in Figs. 10-12, a relatively dense surface film structure is formed on 304-Al coating. The two-phase layer hampers the corrosion attack of HCl solution as a clear and dense two-phase structure exists even after 72 h immersion as shown in Fig. 11. Cr and Al enrichment on the surface film and existence of Cr₂Al₁₃ and Fe₄Al₁₃ as confirmed in EDS mapping and XRD results contribute to the corrosion inhibition of HCl solution.

Based on the analysis above, a corrosion model was proposed to explain the effect of Cr and Ni elements incorporation on microstructure and corrosion behavior of intermetallic coatings, as shown in Fig. 13. When 304–Al intermetallic coating is exposed to HCl solution, galvanic corrosion will occur as two phases co-exist at the interface between coating and electrolyte. Fe₄Al₁₃ phase is preferentially corroded as an anode and Fe²⁺ and

Al3+ cations are released to the electrolyte. Meanwhile, hydrogen gas is evolved from the cathodic site of Cr₂Al₁₃ where the local pH would rise. Corrosion product of iron hydroxide and aluminum hydroxide would precipitate with the immigration of Fe²⁺ and Al³⁺ from anodic to cathodic sites; whereas the low stability of those corrosion products and the presence of chloride in the cathodic sites result in their continuous dissolution. As a consequence, no obvious corrosion product is observed after 72 h immersion in HCl solution as confirmed in Figs. 10–12. With the continuous dissolution of Fe₄Al₁₃ phase by acidic solution, a network structure of Cr₂Al₁₃ is formed at the interface of coating and electrolyte. The formation of network structure provides sufficient protection for the 304-Al coating with no need for the dissolution of uniform layer adjacent to substrate. It is concluded that enrichment of Al and Cr elements and the greater proportion of two-phase layer lead to better corrosion resistance of 304-Al coating. However, defects and cracks in 430-Al coating as shown in Figs. 2 and 11 promote the aggressive ions penetrating and reaching the interface between uniform layer and substrate, and then deteriorate the degradation of intermetallic coating, which compensates the beneficial influence caused by passivity of Cr and Al enrichment on the surface film. There is no doubt that only Fe₂Al₅ layer formed on Fe-Al coating does not show any protection for the substrate after 72 h immersion in HCl solution as shown in Figs. 11 and 12.

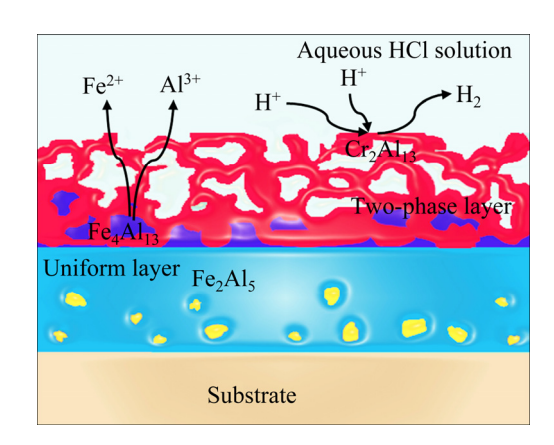


Fig. 13 Model for corrosion of 304–Al coating in 0.5 mol/L HCl solution

4 Conclusions

1) The microstructure and intermetallic phases in the intermetallic coatings on 430-SS, 304-SS and pure Fe were observed by SEM, EDS and EBSD. Overall, all the intermetallic coatings grow intact on the substrates. The intermetallic surface coating is compact and dense on 304-SS substrate, compared with several small cracks

presented on 430-SS substrate and a tongue-like structure on pure Fe. Two-phase layer structure mainly consisting of Cr_2Al_{13} and Fe_4Al_{13} phases was obtained for 430–Al and 304–Al coatings in comparison with only one uniform layer of Fe_2Al_5 for Fe–Al coating. Extra addition of Ni led to greater proportion and crack free of two-phase layer formed on 304-Al coating.

- 2) The corrosion behaviour of three intermetallic coatings was evaluated by the mass loss experiment and electrochemical tests. It is indicated that the corrosion rates of 304-Al, 430-Al and Fe-Al intermetallic coatings were respectively 1.1, 19 and 35 mm/a. An obvious noble shift of open circuit potential was obtained after Cr or both Cr and Ni addition, from -0.68 V for Fe-Al coating to -0.52 V for 430-Al coating and -0.48 V for 304-Al coating. More importantly, around dozens of times enhancement of corrosion resistance was realized by extra addition of Ni to 304-Al coating, where the presence of defects and cracks in 430-Al coating compensated the effective inhibition of two-phase layer to the aggressive media. As comparison, Fe-Al coating could not withstand the attack of high acidic HCl solution.
- 3) The corrosion products were characterized. The presence of two-phase layer is the dominated reason to improve the corrosion resistance of 304–Al coating. The presence of cracks in 430–Al coating provided a pathway for corrosion media penetrating to the substrate and accelerated corrosion rate. Moreover, the presence of Al_{58.5}Fe_{3.2}Cr_{10.3} in the corrosion product of 304–Al coating as confirmed in XRD to some extent enhanced the corrosion resistance. In all, the incorporation of Cr and Ni elements is greatly helpful for improving the corrosion resistance of Fe–Al-based intermetallic coatings.

Acknowledgments

We acknowledge Elodie Sandraz (Nanoengineering Department, University of California, San Diego) for the English revision.

References

- [1] CUI Jin-long, YAO Zhen-dong, CUI Yong-fu, CHENG Fu-peng, XIAO Ting, SUN Hong-liang, TIAN Ru-jin, SUN Jun-cai. Electrochemical properties of tungsten-alloying-modified AISI 430 stainless steel as bipolar plates for PEMFCs used in marine environment [J]. Acta Metallurgica Sinica (English letters), 2016, 29: 920-927
- [2] FANG Xin-xian, ZHOU Heng-zhi, XUE Ya-jun. Corrosion properties of stainless steel 316L/Ni-Cu-P coatings in warm acidic solution [J]. Transactions of Nonferrous Metals Society of China, 2015, 25: 2594-2603.

- [3] ALBRIMI Y A, ADDI A A, DOUCH J, SOUTO R M, HAMDANI M. Inhibition of the pitting corrosion of 304 stainless steel in 0.5 M hydrochloric acid solution by heptamolybdate ions [J]. Corrosion Science, 2015, 90: 522–528.
- [4] TORTORELLI P F, NATESAN K. Critical factors affecting the high-temperature corrosion performance of iron aluminides [J]. Materials Science and Engineering A, 1998, 258: 115–125.
- [5] HOTAŘ A, PALM M, KRATOCHVÍL P, VODIČKOVÁ V, DANIŠ S. High-temperature oxidation behaviour of Zr alloyed Fe₃Al-type iron aluminide [J]. Corrosion Science, 2012, 63: 71–81.
- [6] CINCA N, LIMA C R C, GUILEMANY J M. An overview of intermetallics research and application: Status of thermal spray coatings [J]. Journal of Materials Research and Technology, 2013, 2: 75–86.
- [7] CHU Di, ZHANG Jian-yu, YAO Jin-jin, HAN Yan-qiu, WU Chun-jing. Cu–Al interfacial compounds and formation mechanism of copper cladding aluminum composites [J]. Transactions of Nonferrous Metals Society of China, 2017, 27: 2521–2528.
- [8] ZHANG Zhen-xue, LI Xiao-ying, DONG Han-shan. Plasmanitriding and characterization of FeAl40 iron aluminide [J]. Acta Materialia, 2015, 86: 341–351.
- [9] SINA H, CORNELIUSSON J, TURBA K, IYENGAR S. A study on the formation of iron aluminide (FeAl) from elemental powders [J]. Journal of Alloys and Compounds, 2015, 636: 261–269.
- [10] SHARMA G, AWASTHI R, CHANDRA K. A facile route to produce Fe-Al intermetallic coatings by laser surface alloying [J]. Intermetallics, 2010, 18: 2124-2127.
- [11] SENDEROWSKI C, BOJAR Z, WOLCZYŃSKI W, PAWLOWSKI A. Microstructure characterization of D-gun sprayed Fe–Al intermetallic coatings [J]. Intermetallics, 2010, 18: 1405–1409.
- [12] MOHAMMADKHANI S, JAJARMI E, NASIRI H, VAHDATI-KHAKI J, HADDAD-SABZEVAR M. Applying FeAl coating on the low carbon steel substrate through self-propagation high temperature synthesis (SHS) process [J]. Surface and Coating Technology, 2016, 286: 383–387.
- [13] ZHAO Long-zhi, ZHAO Ming-juan, LI De-ying, ZHANG Jian, XIONG Guang-yao. Study on Fe-Al-Si in situ composite coating fabricated by laser cladding [J]. Applied Surface Science, 2012, 258: 3368-3372.
- [14] AMIRIYAN M, ALAMDARI H D, BLAIS C, SAVOIE S, SCHULZ R, GARIÉPY M. Dry sliding wear behavior of Fe₃Al and Fe₃Al/TiC coatings prepared by HVOF [J]. Wear, 2015, 342–343: 154–162.
- [15] MORRIS D G, MUÑOZ-MORRIS M A, CHAO J. Development of high strength, high ductility and high creep resistant iron aluminide [J]. Intermetallics, 2004, 12: 821–826.
- [16] ZAMANZADE M, VEHOFF H, BARNOUSH A. Cr effect on hydrogen embrittlement of Fe₃Al-based iron aluminide intermetallics: Surface or bulk effect [J]. Acta Materialia, 2014, 69: 210–223.
- [17] CHEVALIER S, JUZON P, PRZYBYLSKI K, LARPIN J P. Water vapor effect on high-temperature oxidation behavior of Fe₃Al intermetallics [J]. Science and Technology of Advanced Materials, 2009, 10: 045006.
- [18] DYBKOV V I. Interaction of 18Cr-10Ni stainless steel with liquid aluminium [J]. Journal of Materials Science, 1990, 25: 3615-3633.
- [19] ZAMANZADE M, BARNOUSH A. Effect of chromium on the electrochemical properties of iron aluminide intermetallics [J]. Corrosion Science, 2014, 78: 223–232.
- [20] ROSALBINO F, CARLINI R, PARODI R, ZANICCHI G, SCAVINO G. Investigation of passivity and its breakdown on

- Fe₃Al–Si and Fe₃Al–Ge intermetallics in chloride-containing solution [J]. Corrosion Science, 2014, 85: 394–400.
- [21] NEGACHE M, TAIBI K, SOUAMI N, BOUCHEMEL H, BELKADA R. Effect of Cr, Nb and Zr additions on the aqueous corrosion behavior of iron-aluminide [J]. Intermetallics, 2013, 36: 73–80.
- [22] MASMOUDI M, MHADHBI M, ESCODA L, SUÑOL J J, KHITOUNI M. Microstructural evolution and corrosion behavior of nanocrystalline FeAl synthesized by mechanical alloying [J]. Journal of Alloys and Compounds, 2016, 657: 330–335.
- [23] PORCAYO-CALDERON J, ARRIETA-GONZALEZ C D, LUNA-RAMIREZ A, SALINAS-BRAVO V M, CUEVAS-ARTEAGA C, BEDOLLA-JACUIENDE A, MARTINEZ-GOMEZ L. Corrosion performance of Fe–Al intermetallic coatings in 1.0 M NaOH solution [J]. International Journal of Electrochemical Science, 2013, 8: 12205–12218.
- [24] ZHU Xiao-lin, YAO Zheng-jun, GU Xue-dong, CONG Wei, ZHANG Ping-ze. Microstructure and corrosion resistance of Fe–Al intermetallic coating on 45 steel synthesized by double glow plasma surface alloying technology [J]. Transactions of Nonferrous Metals Society of China, 2009, 19: 143–148.
- [25] HARACH D J, VECCHIO K S. Microstructure evolution in metal-intermetallic laminate (MIL) composites synthesized by reactive foil sintering in air [J]. Metallurgical and Materials Transactions A, 2001, 32: 1493–1505.
- [26] ZHANG Bao-hong, CONG Wen-bo, YANG Ping. Electrochemistry of metal: Corrosion and protection [M]. Beijing: Chemical Industry Press, 2011. (in Chinese)
- [27] WANG Y, VECCHIO K S. Microstructure evolution in Fe-basedaluminide metallic-intermetallic laminate (MIL) composites [J]. Materials Science and Engineering A, 2016, 649: 325–337.
- [28] KHORUZHA V G, KORNIENKO K E, PAVLYUCHKOV D V, GRUSHKO B, VELIKANOVA T Y. The Al-Cr-Fe phase diagram. I: Phase equilibria at subsolidus temperatures over composition range 58-100 at.% Al [J]. Powder Metallurgy and Metal Ceramics, 2011, 50: 83-97.
- [29] WANG Y, VECCHIO K S. Microstructure evolution in a martensitic 430 stainless steel-Al metallic-intermetallic laminate (MIL) composite [J]. Materials Science and Engineering A, 2015, 643: 72-85.
- [30] BLOBAUM K J, van HEERDEN D, GAVENS A J, WEIHS T P. Al/Ni formation reactions: Characterization of the metastable Al₉Ni₂ phase and analysis of its formation [J]. Acta Materialia, 2003, 51: 3871–3884.
- [31] MURAKAMI K, NISHIDA N, OSAMURA K, TOMOTA Y, SUZUKI T. Aluminization of high purity iron and stainless steel by powder liquid coating [J]. Acta Materialia, 2004, 52: 2173–2184.
- [32] YANG C W, WILLIAMS D B, GOLDSTEIN J J. A revision of the Fe-Ni phase diagram at low temperatures (< 400 °C) [J]. Journal of Phase Equilibria, 1996, 17: 522–531.
- [33] OFORKA N C, ARGENT B B. Thermodynamics of Ni-Cr-Al alloys [J]. Journal of the Less Common Metals, 1985, 114: 97–109.
- [34] HUAPE-PADILLA E, SÁNEHCEZ-CARRILLO M, FLORES RIOS J P, ESPINOSA-MEDINA M A, BAUTISTA-MARGULIS R G, FERRER-SÁNCHEZ M I, CARBAJAL-DELA T G, BEJAR-GÓMEZ L, CHACÓN-NAVA J G, MARTÍNEZ-VILLAFAÑE A. Corrosion study of Fe-Al intermetallic alloys in simulated acid rain [J]. International Journal of Electrochemical Science, 2015, 10: 2141-2154.

- [35] de CRISTOFARO N, FRANGINI S, MIGNONE A. Passivity and passivity breakdown on a β-FeAl intermetallic compound in sulphate and chloride containing solutions [J]. Corrosion Science, 1996, 38: 307–315.
- [36] LÓPEZ M F, ESCUDERO M L. Corrosion behaviour of FeAl-type intermetallic compounds [J]. Electrochimica Acta, 1998, 43: 671–678
- [37] WU Liang, HE Yue-hui, JIANG Yao, ZENG Yi, XIAO Yi-feng, NAN Bo. Effect of pore structures on corrosion resistance of porous Ni₃Al intermetallics [J]. Transactions of Nonferrous Metals Society of China, 2014, 24: 3509–3516.
- [38] CAO Chu-nan, ZHANG Jian-qing. An introduction to electrochemical impedance spectroscopy [M]. Beijing: Science Press, 2002. (in Chinese)
- [39] VERDIAN M M, RAEISSI K, SALEHI M. Corrosion resistance of HVOF-sprayed Ni₂Si intermetallic coatings in hot H₂SO₄ medium [J]. Surface and Coatings Technology, 2014, 240: 70–75.
- [40] OLSSON C O A, LANDOLT D. Passive films on stainless steels: Chemistry, structure and growth [J]. Electrochimica Acta, 2003, 48: 1093–1104.
- [41] YANG W P, COSTA D, MARCUS P. Resistance to pitting and chemical composition of passive films of a Fe-17%Cr alloy in chloride-containing acid solution [J]. Journal of the Electrochemical Society, 1994, 141: 2669–2676.
- [42] HAMM D, OLSSON C O A, LANDOLT D. Effect of chromium content and sweep rate on passive film growth on iron-chromium alloys studied by EQCM and XPS [J]. Corrosion Science, 2002, 44: 1009–1025
- [43] WOLFF I M, IORIO L E, RUMPF T, SCHEERS P V T, POTGIETER J H. Oxidation and corrosion behaviour of Fe-Cr and Fe-Cr-Al alloys with minor alloying additions [J]. Materials Science and Engineering A, 1998, 241: 264-276.
- [44] TROSELIUS L. Polarization performance of stainless steels in H₂SO₄ and HCl [J]. Corrosion Science, 1971, 11: 473–484.
- [45] NINGSHEN S, SAKAIRI M, SUZUKI K, UKAI S. The corrosion resistance and passive film compositions of 12% Cr and 15% Cr oxide dispersion strengthened steels in nitric acid media [J]. Corrosion Science, 2014, 78: 322–334.
- [46] WANG S G, HUANG Y J, SUN M, LONG K, ZHANG Z D. Electrochemical corrosion of bulk nanocrystalline aluminum in acidic sodium sulfate solutions at room temperature [J]. The Journal of Physical Chemistry C, 2015, 119: 9851–9859.
- [47] VEYS D, RAPIN C, LI X, ARANDA L, FOURNÉE V, DUBOIS J M. Electrochemical behavior of approximant phases in the Al-(Cu) -Fe-Cr system [J]. Journal of Non-Crystalline Solids, 2004, 347: 1-10
- [48] KANG Y W, ZHOU C G, GONG S K, XU H B. Electrochemical behavior of low-pressure plasma-sprayed Al-Cu-Fe-Cr quasicrystalline coating [J]. Vacuum, 2005, 148: 148–154.
- [49] BARTHÉS-LABROUSSE M G, BENI A, SCHMUTZ P, DUBOIS J M, BELIN-FERRÉ E. Complex metallic alloys: Fundamentals and applications [M]. Weinheim: Wiley-VCH Verlag GmbH & Co. KGaA, 2011.
- [50] BENI A, OTT N, URA-BINĆZYK E, RASINSKI M, BAUER B, GILLE P, ULRICH A, SCHMUTZA P. Passivation and localised corrosion susceptibility of new Al-Cr-Fe complex metallic alloys in acidic NaCl electrolytes [J]. Electrochimica Acta, 2011, 56: 10524-10532.

Fe-Al 基金属间铝化合物层在酸性条件下的显微组织演变和腐蚀行为

刘文娟1, 王 宇2, 戈宏彬1, 李 莉3, 丁 毅1, 孟令刚4, 张兴国4

- 1. 南京工业大学 材料科学与工程学院,南京 210009;
 - 2. 中北大学 材料科学与工程学院,太原 030051;
- 3. 南京工业大学 化学与分子工程学院,南京 211800;
- 4. 大连理工大学 材料科学与工程学院, 大连 116024

摘 要:采用压力辅助固态扩散结合技术在 430 (Fe-Cr)和 304 (Fe-Cr-Ni)不锈钢基体上制备两种 Fe-Al 基金属间铝化合物层,并与在纯铁上制备的铝化合物层进行比较。采用 SEM、EDS 和 EBSD 分析铝化合物层的显微组织和存在的金属间化合物物相。Al 和基体发生相互扩散,生成在 Fe₄Al₁₃基体上弥散分布的 Cr₂Al₁₃ 网状结构。采用 失重实验、OCP、Tafel 曲线和 EIS 实验研究金属间化合物层在 0.5 mol/L 盐酸溶液中的腐蚀行为。结果表明,与纯铁上的铝化合物层相比,同时添加 Cr 和 Ni 后,304 不锈钢上铝化合物层的耐蚀性提高了十几倍,而 430 不锈钢铝化合物层中裂缝的存在使得腐蚀介质渗透至基体,提高了腐蚀速率。此外,采用 XRD 分析腐蚀产物。结果表明,Cr 和 Ni 的添加能促进耐蚀相的形成,从而提高不锈钢上金属间铝化合物层的耐蚀性。

关键词: 金属间化合物; 铁铝化合物; 不锈钢; 盐酸; 腐蚀

(Edited by Wei-ping CHEN)